ISSN 1024-8560, Atmospheric and Oceanic Optics, 2025, Vol. 38, No. 4, pp. 464–472. © Pleiades Publishing, Ltd., 2025.
Russian Text © The Author(s), 2025, published in Optika Atmosfery i Okeana.

OPTICAL MODELS AND DATABASES

Adjustment of the Power of Model Emissions of Anthropogenic Atmospheric Pollution Sources Based on Measurement Data and Adjoint Problem Methods

P. N. Antokhin[a, b, *], A. V. Penenko[b, c], M. Yu. Arshinov[a], B. D. Belan[a], and A. V. Gochakov[d]

[a] *V.E. Zuev Institute of Atmospheric Optics, Siberian Branch, Russian Academy of Sciences, Tomsk, 634055 Russia*
[b] *Russian State Hydrometeorological University, St. Petersburg, 192007 Russia*
[c] *Institute of Computational Mathematics and Mathematical Geophysics, Siberian Branch, Russian Academy of Sciences, Novosibirsk, 630090 Russia*
[d] *Siberian Regional Hydrometeorological Research Institute, Novosibirsk, 630090 Russia*
**e-mail: apn@iao.ru*

Received November 1, 2024; revised January 10, 2025; accepted January 14, 2025

Abstract—The prediction of the level of air pollution by gaseous and aerosol constituents in cities becomes increasingly significant in view of their serious negative impact on public health and growing ecological risks. The article presents an approach to estimating and adjusting the emission power of anthropogenic sources based on direct and inverse modeling. The WRF-Chem model was used as a direct simulation tool, and the IMDAF system developed by the authors was used for inverse simulation. The results of direct simulation provided data on meteorological fields and the distribution of admixtures necessary for solving adjoint problems. The use of the adjoint problem method made it possible to calculate a correction factor that determines how much the power of sources that fall into the sensitivity zone should be changed to achieve the best agreement with measurements. Our approach can be used to improve the prediction of air quality, refine the inventories of anthropogenic emissions, and develop the strategies for reducing the ecological risks on global and regional scales.

Keywords: numerical modeling, inverse modeling, adjoint problem, emission source
DOI: 10.1134/S1024856025700319

INTRODUCTION

The problem of predicting the level of urban air pollution by gaseous and aerosol constituents is becoming increasingly important due to their negative impact on public health and growing environmental risks [1]. This is manifested most significantly under unfavorable weather conditions such as heat or cold waves. Global and mesoscale chemical transport models (CTMs) are actively used for predicting air quality [2, 3]. A high-quality prediction of the atmospheric pollution level requires actual data on emissions of gaseous and aerosol constituents. Both global databases, such as the Emissions Database for Global Atmospheric Research (EDGAR) [4], and regional databases, such as the emission inventory developed by the Netherlands Organization for Applied Scientific Research (TNO) [5], are actively used nowadays to specify the emission sources. However, these databases have relatively low (0.1°) spatial resolution and time-limited relevance. In addition, they may bear large errors when used to estimate emissions [6], so that pollution forecasts can deviate from the actual measurement data.

Attempts to bring simulations and measurements into a closer agreement pose the problem of refining the emission sources. This can be done using two approaches: "bottom-up" and "top-down." The first approach is aimed to refine the emission inventory, using data on the activity of population, industrial emissions, statistical data on the energy consumption, and different coefficients, describing the contribution and time dynamics of an emission source. In the second approach, the emission source inventories are created using pollutant data from measurement stations, mobile laboratories, and remote sensing. At present, works employing the bottom-up approach are many and include [4, 7]. However, this approach is fraught with a number of problems, associated with the large inaccuracies in the available statistical data on emission sources, coefficients of emission factors, and their strong spatiotemporal variations. Also of note is that the publications of statistical data are delayed in time by one to two years. Taking into account the aforesaid, the top-down approach is pref-

erable, because it makes it possible to use the inverse modeling to refine the emission sources and to bring the simulation results into a closer agreement with measurement data.

A great number of approaches were suggested to date to refine the spatiotemporal distribution of emission sources, based on inverse modeling [8]. The development of inverse modeling methods in CTMs had the consequence that the top-down approach had been one of the main tools in solving this kind of problem [9, 10]. It is primarily used to refine the emission sources of passive tracers or minor gas constituents of the atmosphere, which can be referred to the them (SO_2, CO, CO_2, CH_4, and NO_x); this approach comprises the following methods: mass balance [11–13], back trajectories [14], adjoint problem [15–20] based on the Bayes estimation theory [21, 22], ensemble Kalman filter [23–25], four-dimensional variational approach (4DVAR) [26–28], and the adaptive nudging method [29].

The purpose of this work is to create and test a technique for refining the power of the emission sources on the basis of the top-down approach based on the solution of the adjoint problem for the two-dimensional advection-diffusion model IMDAF (Inverse Modeling and Data Assimilation Framework). It is a simplified modification of an approach based on the sensitivity operators and ensembles of adjoint problem solutions [19, 20].

MATERIALS AND METHODS

In our approach, we used two models: WRF-Chem v.4.2 [3] (the model version will be omitted in the text below) for a direct modeling of variations in the pollutant concentrations, and the IMDAF model for correcting the data on emission sources, computationally more efficient owing to simplifications in the description of admixture transport processes in the atmosphere. The choice of this scheme stems from the need to reduce the computation expenses, since the use of a detailed model in inverse modeling problems, requiring multiple solution of forward and adjoint problems, may consume significant computational resources.

We will compare qualitatively our method with popular approaches to inverse modeling, i.e., 3DVAR and 4DVAR. In classical 4DAVR methods (with weak constraints) the problem of minimization of the objective functional is usually solved iteratively. In our approach, we use expressions that directly relate the powers of the sources with measurements, so the correction algorithm is iteration-free. Instead of the sequential solution of one forward and one adjoint problem in each 4DVAR iteration, this algorithm requires a solution of adjoint problems for each considered element of the measurement data. These calculations are independent of each other and can be efficiently parallelized. Classical 3DVAR-type algorithms do not construct the estimates of the source functions, but, rather, refine the state function directly, so the results from their work are difficult to use as input parameters of the sources for the WRF-Chem model.

Problem Formulation of Inverse Modeling

We will consider the spatiotemporal domain $\bar{W}_T = \bar{W} \times [0, T]$, where $\bar{W}$ is a three-dimensional spatial domain. A combination of two models is used in the approach suggested here. Direct problems are solved using WRF-Chem, i.e., a nonlinear integrated model, which ensures a high accuracy, but requires large computational resources when used to refine the sources on the basis of measurements. The distribution of the concentration fields obtained using the WRF-Chem model will be denoted through $\varphi = \bar{\varphi}[\bar{r}]$, where $\bar{r}(\mathbf{x}, t)$ is the function of the sources distributed in $\bar{W}_T$. In addition, we defined the measurement operator $\bar{H}_m(\varphi)$, which transforms the concentration distribution into measured quantities:

$$\bar{H}_m(\varphi) = \langle \bar{h}_m, \varphi \rangle_{\bar{W}_T}, \tag{1}$$

where $\bar{h}_m$ is the weight function of a measurement; and $\langle\ \rangle$ means a scalar product. For any $a(x, t)$ and $b(x, t)$, the scalar product is defined as

$$\langle a, b \rangle_{\bar{W}_T} = \int_0^T \int_{\bar{W}} a(x, t)\, b(x, t)\, dxdt. \tag{2}$$

For instance, in the case of a point measurement carried out at the point with the coordinates $(x_m, y_m, z_m, t_m) \in \bar{W}_T$ the weight function has the form

$$\begin{aligned} &\bar{h}_m(x, y, z, t) \\ &= \delta(x - x_m)\delta(y - y_m)\delta(z - z_m)\delta(t - t_m), \end{aligned} \tag{3}$$

where δ is the delta function.

Let us have M measurements at the points $(x_m, y_m, z_m, t_m) \in \bar{W}_T$ with the values

$$\begin{aligned} I_m &= \langle \bar{h}_m, \varphi \rangle_{\bar{W}_T} \\ &= \langle \delta(x - x_m)\delta(y - y_m)\delta(z - z_m)\delta(t - t_m), \varphi \rangle. \end{aligned} \tag{4}$$

We assume that the sources can be only ground-based:

$$\bar{r}(x, y, z, t) = \begin{cases} 0 & z > 0; \\ r(x, y, z, t) & z = 0. \end{cases} \tag{5}$$

To refine the values of sources, we will consider a spatially two-dimensional model in the domain $\Omega_T = \Omega \times [0, T]$, where Ω is the two-dimensional spatial domain. In this domain, we will define a mathematical model of the type of advection-diffusion of a

passive admixture that describes the admixture transport in the atmosphere:

$$\frac{\partial \varphi}{\partial t} - \nabla\left(\mathrm{diag}(\boldsymbol{\mu})\nabla\varphi - \mathbf{u}\varphi\right) = f + r, \quad (\mathbf{x}, t) \in \Omega_T; \quad (6)$$

$$\mathbf{n}\left(\mathrm{diag}(\boldsymbol{\mu})\nabla\varphi\right) + \beta\varphi = \alpha, \quad (\mathbf{x}, t) \in \Gamma^{\mathrm{out}} \subseteq \delta\Omega_T; \quad (7)$$

$$\varphi = \alpha, \quad (\mathbf{x}, t) \in \Gamma^{(\mathrm{in})} \subseteq \delta\Omega_T; \quad (8)$$

$$\varphi = \varphi^0, \quad \mathbf{x} = \Omega, \quad t = 0, \quad (9)$$

where $\varphi(\mathbf{x}, t)$ is the state function designating the concentrations of the substances under consideration at the point, $(\mathbf{x}, t) \in \Omega_T$; $\mathbf{u}(\mathbf{x}, t) \in R^2$ is the transport velocity; $\boldsymbol{\mu}(\mathbf{x}, t) \in R^2$ is the vector of the diffusion coefficients; diag(μ) is the matrix with the vector $\mathbf{x}$ on its diagonal; r is an unknown source function; α is the parameter of boundary conditions; Γ^{out} and Γ^{in} are the parts of the domain boundary where the transport velocity is either zero or directed outwards/inwards from/to the domain. A priori (background) values of the sources f and initial data φ^0 are specified. The task of determining the functions φ in Eqs. (1)–(4) from known r and V is called direct. Its solution is denoted through $\varphi[r]$. Then, for any $r^{(2)}$, and $r^{(1)}$ the following sensitivity relationship holds [30]:

$$\left\langle S[h],\, r^{(2)} - r^{(1)} \right\rangle = \left\langle h,\, \varphi[r^{(2)}] - \varphi[r^{(1)}] \right\rangle, \quad (10)$$

where the sensitivity functions $S[h]$ are calculated using the solution of adjoint problem with the right-hand side h. The measurement operator is defined similar to Eq. (4):

$$H_m(\varphi) = \left\langle h_m,\, \varphi \right\rangle_{\Omega_T}, \quad (11)$$

where h_m is the weight function of measurement;

$$\left\langle a,\, b \right\rangle_{\Omega_T} = \int_0^T \int_\Omega a_l(x, t)\, b_l(x, t)\, dxdt. \quad (12)$$

In the case where measurement is carried out at the point with the coordinates $(x_m, y_m, t_m) \in \Omega_T$, the weight function of measurement

$$h_m(x, y, t) = \delta(x - x_m)\,\delta(y - y_m)\,\delta(t - t_m). \quad (13)$$

Let us consider a source as a set of point sources constant in time, namely:

$$r = \sum_{s=a}^{R} r_{(s)}\,\delta(x - x_{(s)})\,\delta(y - y_{(s)}), \quad r_{(s)} > 0, \quad (x_{(s)}, y_{(s)}) \in \Omega, \quad (14)$$

where $x_{(s)}$ and $y_{(s)}$ are the coordinates of the sth point source; and $r_{(s)}$ is the source power. Assume that the correction is only required for the powers $\{r_{(s)}\}$. Then,

$$\sum_{s=1}^{R} (r_{(s)}^{(2)} - r_{(s)}^{(1)}) \left\langle S[h],\, \delta(x - x_{(s)})\,\delta(y - y_{(s)}) \right\rangle = \left\langle h,\, \varphi[r^{(2)}] - \varphi[r^{(1)}] \right\rangle. \quad (15)$$

Suppose that M measurements are available at the points $(x_m, y_m, t_m) \in \Omega_T$ with the values I_m. Then we have M identities

$$\sum_{s=1}^{R} (r_{(s)}^{(2)} - r_{(s)}^{(1)}) \left\langle S[h],\, \delta(x - x_{(s)})\delta(y - y_{(s)}) \right\rangle = \left\langle h_m,\, \varphi[r^{(2)}] \right\rangle - \left\langle h_m,\, \varphi[r^{(1)}] \right\rangle. \quad (16)$$

Assuming

$$I_m = \left\langle h_m,\, \varphi[r^{(2)}] \right\rangle_{\Omega_T}, \quad (17)$$

we derive the system of equations

$$\sum_{s=1}^{R} (r_{(s)}^{(2)} - r_{(s)}^{(1)}) \left\langle S[h_m],\, \delta(x - x_{(s)})\,\delta(y - y_{(s)}) \right\rangle = I_m - \left\langle h_m,\, \varphi[r^{(1)}] \right\rangle. \quad (18)$$

If, for example, we assume that all powers are similarly underestimated or overestimated, then we obtain the correction coefficient

$$r_{(s)}^{(2)} = \rho r_{(s)}^{(1)}, \quad (19)$$

$$(\rho - 1)\sum_{s=1}^{R} r_{(s)}^{(1)} \left\langle S[h_m],\, \delta(x - x_{(s)})\,\delta(y - y_{(s)}) \right\rangle = I_m - \left\langle h_m,\, \varphi[r^{(1)}] \right\rangle, \quad (20)$$

$$\rho = 1 + \frac{I_m - \left\langle h_m,\ \varphi[r^{(1)}] \right\rangle}{\sum_{s=1}^{R} r_{(s)}^{(1)} \left\langle S[h_m],\ \delta(x - x_{(s)})\,\delta(y - y_{(s)}) \right\rangle}. \quad (21)$$

Data Preparation for Numerical Experiment

To conduct numerical experiments, we should specify the distribution of meteorological parameters (wind speed and direction, turbulence coefficient), as well as the initial and boundary conditions for the gas constituents. These data were obtained from direct WRF-Chem simulation from September 1 to 7, 2020. The calculations were performed for two domains in the Lambertian projection. The first coarse domain was 95 × 100 × 21 (the number of cells) (50.13°–70.5° N, 16.7°–70.8° E) with a resolution of 27 km; and the second domain was 145 × 106 × 21 with a resolution of 9 km (54.1°–65.8° N, 24.4°–44.5° E).

The calculations were performed using the following parameterizations: Morrison for microphysics; RRTMG for longwave radiation; RRTMG for shortwave radiation; Noah for the model of the surface;

Mellor-Yamada-Janjic for the planetary boundary layer; and Grell 3D for clouds.

The WRF-Chem model was used for testing in the passive tracer transport mode. As a tracer, we used sulfur dioxide (SO_2), an important indicator of atmospheric processes in the Arctic and tracer of the transport of pollutants and their sources. The participation of sulfur dioxide in the formation of sulfate aerosols influences the climate and radiation balance, and acid precipitation dangers ecosystems. The use of SO_2 as a tracer in the models helps to study the transport dynamics and chemical conversions of atmospheric constituents, which makes it an important component in climatic and ecological studies.

The model was started using NCEP FNL (Final) Operational Global Analysis data [31] with a resolution of 0.25° × 0.25°. The initial and boundary conditions for the air chemical composition were set to zero. The anthropogenic SO_2 emissions were specified at the first five altitude levels from the surface with the coefficients 0.05, 0.6, 0.2, 0.15, and 0.05 using the EDGAR v.4.3.2 database. In the research area, the altitudes of 37, 110, 208, 322, and 440 m above the surface correspond to the first five model levels.

Arkhangelsk (64.60° N, 40.73° E) was chosen as the measurement site for estimating the modeling quality and comparing the results. Two-dimensional IMDAF model version was used in our work; therefore, an optimal altitudinal averaging range should be chosen to compile the input data. This averaging interval is determined by task-specific requirements and can vary in a wide range, depending on specific features of turbulent mixing and pollutant dispersal. We tested a few altitude ranges, and for each took average meteorological parameters and gas composition. This made it possible to take into account the specific features of the distribution of the meteorological parameters and of the pollutant concentration, yet preserving the computation efficiency of the model.

The powers and locations of emission sources in the IMDAF model were specified using the same set of sources as in the direct WRF-Chem modeling. As a consequence, the direct and inverse simulation results were matched and could be efficiently used to refine the emissions.

The results of the WRF-Chem calculations, without changes to the powers of pollutant sources, were used to compile the data of virtual measurements – spatiotemporal time series. The spatial measurements comprised a 3 × 3 square of grid points, with the central one being closest to the coordinates of Arkhangelsk (64.60° N, 40.73° E). The time series for this point comprised 10 measurements with a step of 1 h, starting from 07:00 LT on September 4, 2020. These data were compiled for the altitude averaging ranges 0–100, 0–250, 0–500, and 0–1000 m.

RESULTS AND DISCUSSION

Single Pollution Source

The first series of the numerical experiments was aimed at refining the power of a single emission source that fell within the sensitivity zone of our method. The calculations were performed on the main and nested domains for two altitude averaging ranges: 0–250 and 0–500 m.

The comparison of results from direct simulation performed using simplified two-dimensional model IMDAF with the WRF-Chem data showed good agreement (Fig. 1). The figure presents the calculations performed at 09:00 GMT on September 4, 2020. For clarity, the area under study where, the source and measurement site are located is bounded by the coordinates 61°–65° N, 36°–43° E.

Despite certain discrepancies (see Fig. 1), the model successfully reproduces both the main spatial and temporal characteristics of the admixture transport, indicating its adequacy for the problems of the given type. However, transition to a two-dimensional model unavoidably involves certain simplifications associated with averaging of the meteorological parameters, which leads to partial losses in accuracy of reproducing local processes and vertical exchange.

After making sure that the direct problem is solved correctly, we analyzed the results of numerical experiment. Estimates of the correction coefficient of the source power for this numerical experiment are presented in Table 1 for areal data and time series (compilation of these times series is described above). The first column shows how strongly the source power was changed relative to the initial specified power. Values in table cells show the coefficient by which the used source power should be multiplied to minimize the deviation from observations. If the coefficient is 2.1 ± 0.2 for the main domain and altitude of 0–250 m (case of $0.5r(x, y)$), this means that the source power should be increased by a factor of 2.1 in order to achieve the coincidence with measurements.

In the case where the source power was not changed, the IMDAF model showed a good agreement with the observations for both the main and nudged domains. The correction coefficient was unity. Its insignificant deviations from unity were observed for the nudged domain; however, they were within the root-mean-square (rms) deviation. The calculations on the main domain showed that, as the source power decreases to 50% of the initial one, the correction coefficient calculated using the spatial data proportionally grew to 2.11 and 2.01 in the altitude ranges 0–250 and 0–500 m, respectively. For the nudged domain, the coefficients were found to be somewhat larger: 2.42 and 2.01, respectively. For the time series, the ρ_m behaved similarly, but the rms deviation was lower. After the power fivefold increases relative to the initial one, the ρ_m is determined much better, indi-

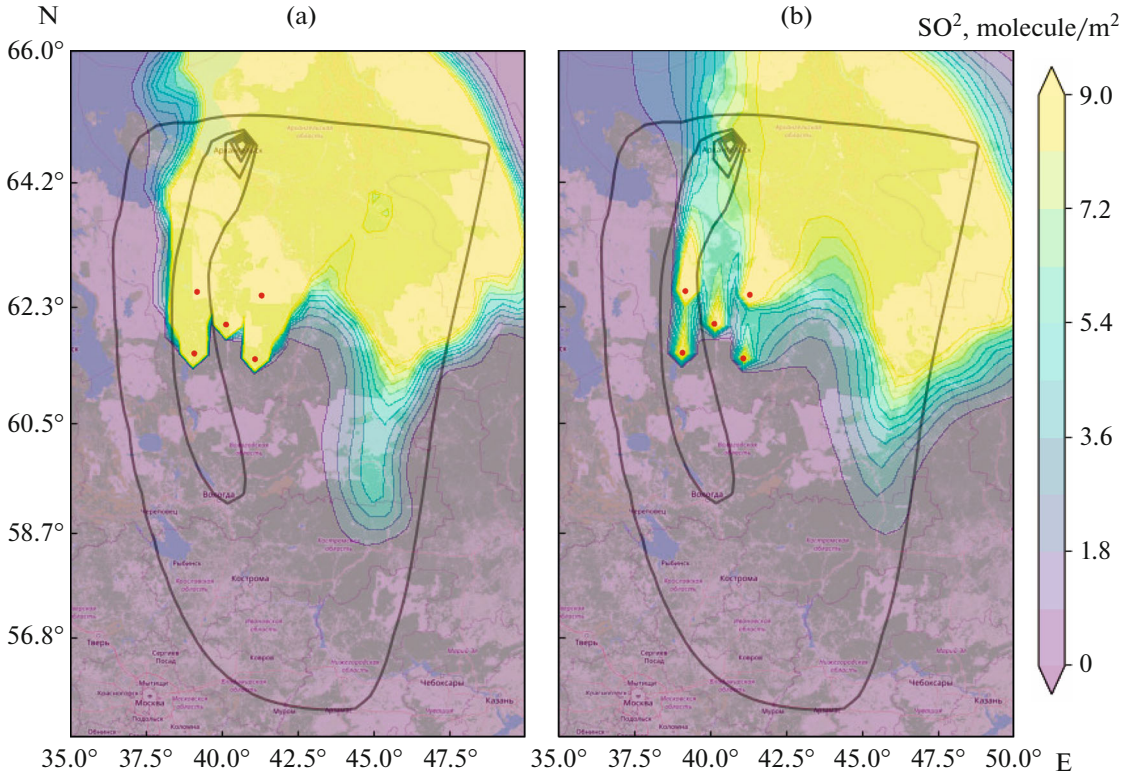

Fig. 1. Calculations of the SO_2 concentrations with the averaging layer of 0–250 m for the main domain, using (a) WRF-Chem and (b) IMDAF models; contour line indicates the sensitivity zone; locations of the sources are indicated by red circles.

cated by a quite low rms deviation. As a result of the numerical experiments performed, our approach demonstrated a possibility of a power correction for a single source based on results of inverse simulation using the IMDAF model.

Few Point Pollution Sources

The calculations of the correction coefficient for a few emission sources (Table 2) show that the IMDAF model, as for a single source, estimated the changes adequately. The rms deviation decreased after the sources increased in number. For instance, in the case

Table 1. Coefficients of retrieval of the power of a single pollution source

Source power	Averaging height, m			
	main domain		nudged domain	
	0–250	0–500	0–250	0–500
$0.5r(x, y)$	2.11 ± 0.20 *2.01 ± 0.11*	2.05 ± 0.74 *2.10 ± 0.08*	2.42 ± 0.48 *2.01 ± 0.28*	2.10 ± 0.45 *2.10 ± 0.36*
$r(x, y)$	1.02 ± 0.10 *1.01 ± 0.05*	1.00 ± 0.374 *1.02 ± 0.04*	1.20 ± 0.24 *1.01 ± 0.14*	1.12 ± 0.22 *1.13 ± 0.18*
$5r(x, y)$	0.22 ± 0.02 *0.20 ± 0.01*	0.20 ± 0.07 *0.21 ± 0.01*	0.20 ± 0.05 *0.21 ± 0.03*	0.20 ± 0.04 *0.20 ± 0.04*

Here and in tables below entries in nonitalic are for the spatially distributed data; and entries in italic are for the time series.

Table 2. Coefficients of retrieval of powers of few pollution sources

Source power	Averaging height, m			
	main domain		nudged domain	
	0–250	0–500	0–250	0–500
$0.5r(x, y)$	2.10 ± 0.05 *2.01 ± 0.04*	2.01 ± 0.10 *2.00 ± 0.02*	2.06 ± 0.03 *2.05 ± 0.05*	2.11 ± 0.11 *2.02 ± 0.04*
$r(x, y)$	1.01 ± 0.03 *1.02 ± 0.02*	1.02 ± 0.04 *1.01 ± 0.01*	1.03 ± 0.01 *1.02 ± 0.02*	1.10 ± 0.06 *1.01 ± 0.02*
$5r(x, y)$	0.21 ± 0.01 *0.20 ± 0.01*	0.20 ± 0.01 *0.20 ± 0.01*	0.21 ± 0.00 *0.20 ± 0.01*	0.20 ± 0.01 *0.20 ± 0.01*

Table 3. Sensitivity of the method for correcting the power of a single point source to changes in the averaging height

Source power	Averaging height, m			
	main domain		nudged domain	
	0–100	0–1000	0–100	0–1000
$0.5r(x, y)$	1.90 ± 99.96 *4.03 ± 1.34*	1.81 ± 0.10 *1.80 ± 0.09*	0.50 ± 301.48 *0.60 ± 0.32*	2.53 ± 0.39 *2.0 ± 0.51*
$r(x, y)$	1.00 ± 49.98 *2.00 ± 0.67*	0.90 ± 0.05 *0.90 ± 0.05*	0.32 ± 150.74 *0.31 ± 0.16*	1.20 ± 0.19 *1.0 ± 0.25*
$5r(x, y)$	0.20 ± 10.00 *0.40 ± 0.13*	0.20 ± 0.01 *0.20 ± 0.01*	0.05 ± 30.15 *0.06 ± 0.03*	0.20 ± 0.04 *0.20 ± 0.05*

of $0.5r(x, y)$, the rms deviation of the spatial data decreased from 0.74 (a single source) to 0.10 (a few sources) for the main domain when the averaging height was 0–500 m. The rms decrease was found to be from a factor of 2 to 10 on the whole, and up to a factor of 4 for the nudged domain.

Estimate of How the Method of Correcting the Power of a Single Source is Sensitive to Change in Averaging Height

Calculations for a single source with zero initial and boundary conditions were carried out to check the sensitivity of the method for correcting the power of the emission source to the averaging height. We considered two layers: 0–100 m, where the information can be lost due to the mixing height, and 0–1000 m, were background concentrations affect. The results of the calculations are presented in Table 3.

From Table 3 we can conclude that the error of the ρ_m estimation sharply increases due to the use of the small averaging range 0–100 m, confirmed by both the coefficient itself and its rms deviation. No unambiguous regular effect due to transition from the main domain to the nudged one could be found. When the layer 0–1000 m was used, the ρ_m estimates for the spatial data were quite close to the specified values and comparable well to those obtained in Table 1. The ρ_m estimates for temporal data demonstrated a good agreement with estimates obtained previously for the nudged domain. The ρ_m estimates for the main domain were unsatisfactory. It can be concluded that the height of the averaging layer should be chosen to be from 250 to 1000 m for the spatial data and up to 500 m for time series to get a correct ρ_m estimate.

Estimate of How the Method for Correcting the Powers of Few Sources is Sensitive to Changes in Averaging Height

The numerical experiments for few emission sources (Table 4) show that the algorithm is successful at compensating for the information losses characteristic for a thin averaging layer, as compared to a single source. For instance, for the main domain at the height of 0–100 m the correction coefficient for the time series was 3.01 ± 0.72 versus 4.03 ± 1.34 for a single source. Significant improvements were also observed for the nudged domain.

Table 4 for the averaging layer 0–1000 m shows that the time series give the most accurate correction coefficients with the least rms deviation. The coefficient is overestimated for a single pollution source and underestimated for few sources. As an example, for the

Table 4. Sensitivity of the method for correcting the powers of few pollution sources to the changes in the averaging height

Source power	Averaging height, m			
	main domain		nudged domain	
	0–100	0–1000	0–100	0–1000
$0.5r(x, y)$	1.72 ± 1.96 *3.01 ± 0.72*	1.90 ± 0.23 *2.00 ± 0.08*	1.11 ± 1.05 *2.25 ± 1.94*	1.72 ± 0.23 *2.00 ± 0.16*
$r(x, y)$	0.86 ± 0.98 *1.50 ± 0.36*	0.95 ± 0.12 *1.00 ± 0.04*	0.56 ± 0.52 *1.13 ± 0.97*	0.86 ± 0.11 *1.00 ± 0.08*
$5r(x, y)$	0.17 ± 0.20 *0.30 ± 0.07*	0.19 ± 0.02 *0.20 ± 0.01*	0.11 ± 0.10 *0.23 ± 0.19*	0.17 ± 0.02 *0.20 ± 0.02*

case of $5r(x, y)$, the coefficient was 2.53 ± 0.39 for a single source and 1.72 ± 0.23 for few sources.

CONCLUSIONS

The calculations performed using model data showed that our approach relying on the correction coefficient for the powers of pollution sources makes it possible to refine the power efficiently and justifiably. However, it should be noted that this approach needs further improvement in order to incorporate the dynamics of the atmospheric boundary layer, the contributions from the daily and weekly behaviors of the powers of emission sources, conversion of chemical substances, the effect of precipitation, and the accuracy of specifying the meteorological parameters. All these are the tasks to be solved in our future research.

FUNDING

The algorithms for the data assimilation and solution of inverse problems for three-dimensional models were developed under the support of the Ministry of Science and higher education of the Russian Federation (Institute of Computational Mathematics and Mathematical Geophysics, Siberian Branch, Russian Academy of Sciences, FWNM-2022-0003). The regional models of the hydrothermodynamics of the atmosphere were configured and the regional scenarios of inverse modeling were specified under the support from the Russian Science Foundation (grant no. 23-77-30008). The data were stored and processed under the support of the Ministry of Science and higher education of the Russian Federation (V.E. Zuev Institute of Atmospheric Optics, Siberian Branch, Russian Academy of Sciences).

CONFLICT OF INTEREST

The authors of this work declare that they have no conflicts of interest.

REFERENCES

1. K. Adams, D. S. Greenbaum, R. Shaikh, A. M. van Erp, and A. G. Russell, "Particulate matter components, sources, and health: Systematic approaches to testing effects," J. Air Waste Manag. Ass. **65**, 544–558 (2015). https://doi.org/10.1080/10962247.2014.1001884
2. A. Mahura, A. Baklanov, R. Makkonen, M. Boy, T. Petaja, H. K. Lappalainen, R. Nuterman, V.-M. Kerminen, S. R. Arnold, M. Jochum, A. Shvidenko, I. Esau, M. Sofiev, A. Stohl, T. Aalto, J. Bai, C. Chen, Y. Cheng, O. Drofa, M. Huang, L. Jarvi, H. Kokkola, R. Kouznetsov, T. Li, P. Malguzzi, S. Monks, M. B. Poulsen, S. M. Noe, Y. Palamarchuk, B. Foreback, P. Clusius, A. Soya, J. She, J. H. Sorensen, D. Spracklen, H. Su, J. Tonttila, S. Wang, J. Wang, T. Wolf-Grosse, Y. Yu, Q. Zhang, W. Zhang, W. Zhang, X. Zheng, S. Li, Y. Li, P. Zhou, and M. Kulmala, "Towards seamless environmental prediction—development of Pan-Eurasian EXperiment (PEEX) modelling platform," Big Earth Data **8**, 189–230 (2024).
3. G. A. Grell, S. E. Peckham, R. Schmitz, S. A. McKeen, G. Frost, W. C. Skamarock, and doi 10.5194/gmd-11-4603-2018B. Eder, "Fully coupled "online" chemistry within the WRF model," Atmos. Environ. **39**, 6957–6975 (2005). https://doi.org/10.1016/j.atmosenv.2005.04.027
4. M. Crippa, D. Guizzardi, F. Pagani, M. Schiavina, M. Melchiorri, E. Pisoni, F. Graziosi, M. Muntean, J. Maes, L. Dijkstra, M. V. Damme, L. Clarisse, and P. Coheur, "Insights into the spatial distribution of global, national, and subnational greenhouse gas emissions in the Emissions Database for Global Atmospheric Research (EDGAR V8.0)," Earth Syst. Sci. Data **16**, 2811–2830 (2024). https://doi.org/10.5194/essd-16-2811-2024
5. J. J. P. Kuenen, A. J. H. Visschedijk, and M. Jozwicka, "Denier Van Der Gon H.A.C. TNO-MACC_II emission inventory; a multi-year (2003–2009) consistent high-resolution European emission inventory for air quality modelling," Atmos. Chem. Phys. **14**, 10963–10976 (2014). https://doi.org/10.5194/acp-14-10963-2014

6. I. Yu. Shalygina, I. N. Kuznetsova, M. I. Nakhaev, D. V. Borisov, and E. A. Lezina, "Emission correction efficiency for calculations in the CHIMERE chemical transport model in the Moscow region," Opt. Atmos. Okeana **33** (6), 441–447 (2020). https://doi.org/10.15372/AOO20200604

7. L. Liu, H. Liu, G. Geng, C. Hong, F. Liu, Y. Song, D. Tong, B. Zheng, H. Cui, H. Man, Q. Zhang, and K. He, "Anthropogenic emission inventories in China: A review," Nat. Sci. Rev. **4**, 834–866 (2017). https://doi.org/10.1093/nsr/nwx150

8. X. Cheng, Z. Hao, Z. Zang, Z. Liu, X. Xu, S. Wang, Y. Liu, Y. Hu, and X. Ma, "A new inverse modeling approach for emission sources based on the DDM-3D and 3DVAR techniques: An application to air quality forecasts in the Beijing–Tianjin–Hebei region," Atmos. Chem. Phys. **21**, 13747–13761 (2021). https://doi.org/10.5194/acp-21-13747-2021

9. I. G. Enting, *Inverse Problems in Atmospheric Constituent Transport* (University Press, Cambridge, 2002). https://doi.org/10.1017/CBO9780511535741

10. B. Sportisse, "A review of current issues in air pollution modeling and simulation," Comput. Geosci. **11**, 159–181 (2007). https://doi.org/10.1007/s10596-006-9036-4

11. R. V. Martin, "Global inventory of nitrogen oxide emissions constrained by space-based observations of NO_2 columns," J. Geophys. Res. **108** (2003). https://doi.org/10.1029/2003jd003453

12. Y. Wang, X. Chen, R. V. Martin, D. G. Streets, Q. Zhang, and T.-M. Fu, "Seasonal variability of NO_x emissions over East China constrained by satellite observations: Implications for combustion and microbial sources," J. Geophys. Res. **112** (2007). https://doi.org/10.1029/2006jd007538

13. Q. Yang, Y. H. Wang, C. Zhao, Z. Liu, I. William, J. Gustafson, and M. Shao, "NO_x emission reduction and its effects on ozone during the 2008 Olympic Games," Environ. Sci. Technol. **45**, 6404–6410 (2011). https://doi.org/10.1021/es200675v

14. A. J. Manning, S. O'Doherty, A. R. Jones, P. G. Simmonds, and R. G. Derwent, "Estimating UK methane and nitrous oxide emissions from 1990 to 2007 using an inversion modeling approach," J. Geophys. Res. **116** (2011). https://doi.org/10.1029/2010jd014763

15. F. Li, F. Hu, and J. Zhu, "Solving the optimal layout problem of multiple industrial pollution sources using the adjoint method," Sci. China: Earth Sci. **35**, 64–71 (2005).

16. M. R. Koohkan, M. Bocquet, Y. Roustan, Y. Kim, and C. Seigneur, "Estimation of volatile organic compound emissions for europe using data assimilation," Atmos. Chem. Phys. **13**, 5887–5905 (2013). https://doi.org/10.5194/acp-13-5887-2013

17. L. Zhang, J. Shao, X. Lu, Y. Zhao, Y. Hu, D. K. Henze, H. Liao, S. Gong, and Q. Zhang, "Sources and processes affecting fine particulate matter pollution over North China: An adjoint analysis of the Beijing APEC period," Sci. Technol. **50**, 8731–8740 (2016). https://doi.org/10.1021/acs.est.6b03010

18. C. Wang, X. An, S. Zhai, Q. Hou, and Z. Sun, "Tracking sensitive source areas of different weather pollution types using GRAPES-CUACE adjoint model," Atmos. Environ. **175**, 154–166 (2018). https://doi.org/10.1016/j.atmosenv.2017.11.041

19. A. Penenko, "Convergence analysis of the adjoint ensemble method in inverse source problems for advection-diffusion-reaction models with image-type measurements," Inverse Prob. Imaging **14**, 757–782 (2020). https://doi.org/10.3934/ipi.2020035

20. A. V. Gochakov, A. V. Penenko, P. N. Antokhin, and A. B. Kolker, "Air pollution modelling in urban environment based on a priori and reconstructed data," IOP Conf. Ser.: Earth Environ. Sci. **211**, 12050 (2018). https://doi.org/10.1088/1755-1315/211/1/012050

21. M. Kopacz, D. J. Jacob, D. K. Henze, C. L. Heald, D. G. Streets, and Q. Zhang, "Comparison of adjoint and analytical Bayesian inversion methods for constraining Asian sources of carbon monoxide using satellite (MOPITT) measurements of CO columns," J. Geophys. Res. **114** (2009). https://doi.org/10.1029/2007jd009264

22. D. D. Lucas, M. Simpson, P. Cameron-Smith, and R. L. Baskett, "Bayesian inverse modeling of the atmospheric transport and emissions of a controlled tracer release from a nuclear power plant," Atmos. Chem. Phys. **17**, 13521–13543 (2017). https://doi.org/10.5194/acp-17-13521-2017

23. M. Bocquet, H. Elbern, H. Eskes, M. Hirtl, R. Zabkar, G. R. Carmichael, J. Flemming, A. Inness, M. Pagowski, J. L. Perez Camano, P. E. Saide, J.R. San, M. Sofiev, J. Vira, A. Baklanov, C. Carnevale, G. Grell, and C. Seigneur, "Data assimilation in atmospheric chemistry models: Current status and future prospects for coupled chemistry meteorology models," Atmos. Chem. Phys. **15**, 5325–5358 (2015). https://doi.org/10.5194/acp-15-5325-2015

24. D. Chen, Z. Liu, J. Ban, and M. Chen, "The 2015 and 2016 wintertime air pollution in China: SO_2 emission changes derived from a WRF-Chem/EnKF coupled data assimilation system," Atmos. Chem. Phys. **19**, 8619–8650 (2019). https://doi.org/10.5194/acp-19-8619-2019

25. T. Dai, Y. Cheng, D. Goto, Y. Li, X. Tang, G. Shi, and T. Nakajima, "Revealing the sulfur dioxide emission reductions in China by assimilating surface observations in WRF-Chem," Atmos. Chem. Phys. **21**, 4357–4379 (2021). https://doi.org/10.5194/acp-21-4357-2021

26. H. Elbern, A. Strunk, H. Schmidt, and O. Talagrand, "Emission rate and chemical state estimation by 4-dimensional variational inversion," Atmos. Chem. Phys. **7**, 3749–3769 (2007). https://doi.org/10.5194/acp-7-3749-2007

27. Y. Niwa, H. Tomita, M. Satoh, R. Imasu, Y. Sawa, K. Tsuboi, H. Matsueda, T. Machida, M. Sasakawa, B. Belan, and N. Saigusa, "A 4D-var inversion system based on the icosahedral grid model (NICAM-TM 4D-Var V1.0). Part 1: Offline forward and adjoint transport models," Geosci. Model Develop. **10**, 1157–1174 (2017).
https://doi.org/10.5194/gmd-10-1157-2017

28. S. Voshtani, R. Menard, T. W. Walker, and A. Hakami, "Use of assimilation analysis in 4D-var source inversion: Observing System Simulation Experiments (OSSEs) with GOSAT methane and hemispheric CMAQ," Atmosphere **14**, 758 (2023).
https://doi.org/10.3390/atmos14040758

29. Y. Hu, M. T. Odman, and A. G. Russell, "Top-down analysis of the elemental carbon emissions inventory in the United States by inverse modeling using Community Multiscale Air Quality Model with Decoupled Direct Method (CMAQ-DDM)," J. Geophys. Res. **114** (2009).
https://doi.org/10.1029/2009jd011987

30. G. I. Marchuk, *Mathematical Simulation in Environmental Problems* (Nauka, Moscow, 1982) [in Russian].

31. NCEP FNL Operational Model Global Tropospheric Analyses, continuing from July 1999.
https://doi.org/10.5065/D6M043C6

Translated by O. Bazhenov

Publisher's Note. Pleiades Publishing remains neutral with regard to jurisdictional claims in published maps and institutional affiliations.
AI tools may have been used in the translation or editing of this article.